



Synthesis of SAPO-34 using the different combinations of four templates by dry gel conversion method

Baljinder Kaur Riyar¹ · Vijay Kumar Agarwal¹

Received: 16 August 2020 / Revised: 13 August 2021 / Accepted: 15 August 2021 / Published online: 21 August 2021
© Associação Brasileira de Engenharia Química 2021

Abstract

One of the reasons for the gigantic interest in SAPO-34 by researchers is to commercialize SAPO-34 effectively by considering the economic, energy, and activity aspects as it has found enormous uses in various industrial applications. The present study focuses on the preparation method named the dry gel conversion method for synthesizing SAPO-34. Four different structure-directing agents (SDA's) (tetraethylammonium hydroxide (TEAOH), triethylamine (TEA), morpholine, diethylamine (DEA)) in different amounts are utilized for the synthesis of SAPO-34 along with alumina, silica, phosphorus precursors. Two sets of a mixed combination of the templates are taken into consideration for SAPO-34, which are TEAOH/TEA/Morpholine/DEA with the molar composition of 0.2/0.4/0.6/0.8 and 0.4/0.2/0.8/0.6, and crystallization time is taken as 3, 5, and 8 h. XRD, FTIR, TPD, nitrogen adsorption, TGA, SEM, EDX, TEM investigated the catalyst's physicochemical properties. For both gel compositions, the pure phase of SAPO-34 is formed at 5 h, with the variation in the intensity of crystallinity. The micropore surface area and external surface area of the prepared catalysts fall in the range of 79–697 m²/g and 44–175 m²/g, respectively.

Keywords SDA's · TEAOH · Morpholine · DEA · TEA · SAPO-34 · Dry gel conversion method

Introduction

Zeolites or molecular sieves are the porous crystalline structure of hydrated silicates of aluminium, silicon, and oxygen atoms. Aluminophosphate (AlPO_{4-n}) molecular sieves were pioneered by Wilson et al. (1982). Later, Lok et al. (1984a, b) synthesized the silicoaluminophosphate (SAPO) zeolite SAPO-34 by silicon incorporation into the AlPO_{4-n} framework, which creates a negative charge in the framework and thus the Brønsted acid sites are formed. The SAPO-34 finds applications in the selective catalytic reduction of NO_x by ammonia (NH₃-SCR) (Fan et al. 2019), carbon-dioxide removal (Ahmad et al. 2019), xenon capture from the air (Wu et al. 2019), N₂/CH₄ separation (Zong and Carreon 2017), methanol to olefins (Bahrami et al. 2018). It is proclaimed to be a catalyst for the conversion of methanol to light olefins, as it is a

non-petroleum route for the mass production of olefins. It possesses CHA topology with eight-membered rings, pore opening of 0.38 nm, and weak acidity, hydrothermal stability, which help induce the selectivity of light olefins (ethene and propene). SAPO-34 gets deactivated quickly due to the deposition of coke. Assorted studies indicate that this setback could be removed by reducing the catalyst size. When, pore length is reduced, it sequentially shortens the residence time of the reactant in the pore. Researchers are striving to ameliorate the lifetime of the catalyst in order to facilitate the commercialization of SAPO-34. The divergent methods used for the preparation of SAPO-34 are: hydrothermal treatment (Valizadeh et al. 2014), dry gel method (Hirota et al. 2010), microwave-assisted (Shalmani et al. 2012), seed-assisted synthetic method (Sun et al. 2020), ultra-sonic pretreatment (Askari and Halladj 2012), ionothermal method (Sánchez-Sánchez et al. 2017). All the acknowledged methods have a considerable impact on crystal size, purity, and morphology. Hydrothermal treatment is the conventional method for synthesizing SAPO-34, though it takes a minimum of 24 h of synthesis time. Many groups have been working on the Dry gel conversion method for the synthesis of zeolites.

✉ Baljinder Kaur Riyar
briyar@ch.iitr.ac.in

¹ Chemical Engineering Department, Indian Institute of Technology Roorkee, Roorkee 247667, Uttarakhand, India

In the dry gel method, the gel is dried before the crystallization stage; thus, the nucleation sites are formed early at much lower supersaturation levels. The dry gel method takes less than half of the time taken by the hydrothermal method to obtain SAPO-34 (Askari et al. 2014; Hirota et al. 2010) and downscales the waste disposal and reactor volume.

Amidst the gelation or the nucleation process, the role of the templates is to systematize the oxide tetrahedra to a particular geometrical structure around itself, which builds the initial building block for the desired structure (Lok et al. 1983). Also, highly siliceous materials are obtained by using organic templates, and it is also associated with the framework charge compensation related to SiO_4 tetrahedra (Vomscheid et al. 1994). One template in the synthesis media may lead to the formation of one molecular sieve framework, and a different template mixture can generate the one desired specific framework. Nucleation and crystal-growth hinged on the interaction of the template with the inorganic species and alkalinity of the solution. Several templates are exercised to make SAPO's and have a peculiar influence on the acidity of the sample (Álvarez-Muñoz et al. 2012). Some of them are tetraethylammonium hydroxide (TEAOH) (Hirota et al. 2010), morpholine (Marchese et al. 1999; Prakash and Unnikrishnan 1994), dipropylamine (DPA) (Fan et al. 2016), triethylamine (TEA) (Wang et al. 2011), diethylamine (DEA) (Liu et al. 2012), N,N,N',N'-tetraethylethane-1,2-diamine (TEEDA) (Nishiyama et al. 2009), piperidine (Dumitriu et al. 1997), and so on. It has been established that TEOH is an ideal template for SAPO-34 (Askari and Halladj 2012; Hirota et al. 2010; Liang et al. 1990; Liu et al. 2016) since it is expensive, which proliferate the production cost of catalyst. The moles of templates change the physicochemical properties and cost of the catalyst, so the work on other templates and the combination of templates is gaining momentum. Multiple studies observed a reduction of crystal size by using a combination of two templates (Rostami et al. 2014; Sedighi et al. 2014; Wang et al. 2012; Ye et al. 2011). Masoumi et al. (2015) and Doan et al. (2019) have successfully synthesized SAPO-34 using three different templates (TEAOH/Morpholine/TEA). A substantial amount of work has been published on TEOH, morpholine, TEA, DEA, and the combination of dual or triple templates in the synthesis of SAPO-34. The number of small nuclei are increased by incorporating a large number of templates, which implies that a large amount of small crystals are developed rather than small number of large crystals. Utilizing different template combinations

is an economical method for the synthesis of SAPO-34 (Doan et al. 2019). However, the literature on the combination of these four templates as SDA for SAPO-34 is limited. Najafi et al. (2014) synthesized SAPO-34 by the hydrothermal treatment method and compared the single template synthesized SAPO-34, using two, three, and four templates (TEAOH/Morpholine/TEA/DEA).

Hitherto, no research has been done on the synthesis of SAPO-34 by combining four templates by the dry gel method. The silica source used by Najafi et al. (2014) was tetraethyl orthosilicate (TEOS). The effect of different silica sources in SAPO-34 was studied by Popova et al. (1998) who reported variations of crystallinity and density of acid sites. In the present study, we aim to synthesize SAPO-34 by the dry gel method. Then the properties of the catalyst samples are analysed by XRD, FTIR, TPD, BET, TGA, SEM, EDX, and TEM.

Materials and methods

Chemicals

All the reagents, aluminium isopropoxide (AIP, $\geq 98\%$ Sigma-Aldrich), phosphoric acid (H_3PO_4 , $> 99\%$, Ranken), LUDOX (40 wt% suspension in H_2O , Sigma-Aldrich), tetraethylammoniumhydroxide (TEAOH, 35 wt% in water, Sigma-Aldrich), diethylamine (DEA, $> 99.5\%$ Sigma-Aldrich), triethylamine (TEA, $> 99.5\%$ Sigma-Aldrich), morpholine ($\geq 99\%$, Sigma-Aldrich) were used without purification. All the chemicals were procured from H. V. Technologies, Dehradun, India.

Preparation of SAPO-34 catalysts

Preparation of SAPO-34 involves two different molar reaction mixture compositions, $1\text{Al}_2\text{O}_3: 1\text{P}_2\text{O}_5: 0.6\text{SiO}_2: 0.2\text{TEAOH}: 0.4\text{TEA}: 0.6\text{Morpholine}: 0.8\text{DEA}: 70\text{H}_2\text{O}$ and $1\text{Al}_2\text{O}_3: 1\text{P}_2\text{O}_5: 0.6\text{SiO}_2: 0.4\text{TEAOH}: 0.2\text{TEA}: 0.8\text{Morpholine}: 0.6\text{DEA}: 70\text{H}_2\text{O}$ in present study. The dry gel conversion method used in the present study is slightly different from the steam-assisted conversion (SAC) and vapor phase transport (VPT). At first, the mixture of aluminiumisopropoxide (AIP), organic templates (Morpholine, TEOH, TEA, DEA), and Millipore water was stirred at room temperature until a homogeneous solution was obtained. Then the silica source (LUDOX) was added while stirring. At last, H_3PO_4 was added dropwise under continuous stirring for an hour. The reaction mixture was aged for 6 h and dried

Table 1 Synthesis conditions of samples

Sample	Relative crystallinity
S-1	21
S-2	100
S-3	39
S-4	78
S-5	84
S-6	19

overnight at 80 °C. The crushed reaction mixture was then transferred to the Teflon lined autoclave with the same amount of Millipore water as the crushed gel and placed in the hot air oven at 180 °C for a certain time (Table 1) under autogenic pressure. Then the recovered solid product was cooled at room temperature. It was washed four to five times by centrifugation with distilled water followed by drying at 110 °C under airflow. The final product was calcined in an air atmosphere at 650 °C for 6 h to remove the organic templates. For comparison, another catalyst is prepared with the molar composition of 1Al₂O₃: 1P₂O₅: 0.6SiO₂: 0.4TEAOH: 0.2TEA: 0.6Morpholine: 0.8DEA: 70H₂O with the crystallization time of 8 h.

Characterization

Powdered X-Ray diffraction (XRD) patterns were recorded with a Bruker D8-Advance X-Ray diffractometer operated at 40 kV and 40 mA, using CuK α radiation ($\lambda = 1.54 \text{ \AA}$) with the angular range between 5 and 50°. XRD patterns determine the phase purity and crystallinity of the samples. The relative crystallinity of the samples was estimated by taking the reference of the most intense peak from all the six samples, so S-2 was taken at $2\theta = 9.8^\circ$. FullProf Suite was used for Rietveld refinement of the obtained diffractograms of the samples. Fourier transform infrared spectroscopy (FT-IR) was conducted on a Perkin Elmer spectrum II with a pellet containing KBr and IR spectra registered in the region of 400–4000 cm⁻¹ at ambient atmosphere with the resolution of 0.5 cm⁻¹. The acidic properties of the catalyst were determined on a Micromeritics Chemisorb 2720; first, the sample was pre-treated at 300 °C for 3 h to remove the water present in the catalyst. At 100 °C, ammonia is adsorbed for 30 min, and then helium was purged for 45 min at 20 mL/min. For the removal of the physically adsorbed ammonia, the samples were kept under helium flow at 100 °C and while the temperature was increased to 700 °C at a rate of 10 °C/min. The nitrogen absorption–desorption measurement was

performed on AutosorbiQ Station 1–Quantchrome instruments. 40 mg of sample was outgassed for 5 h at a temperature of 300 °C. External surface area and micropore volume of SAPO-34 were calculated by the t-plot method. The Density Functional Theory (DFT) method was implemented for the evaluation of pore size distribution. Thermal analysis of the sample was carried out on an EXSTAR TG/DTA 6300 under the following conditions: sample weight 10.5 mg; reference compound, alumina powder; temperature range, 35–900 °C; heating rate 10 °C/min; the atmosphere, flowing air. The surface morphology was determined by scanning electron microscopy (Carl Zeiss Ultra Plus). The composition of the product was evaluated with an energy dispersive x-ray (EDX) attachment equipped with SEM (Carl Zeiss Ultra Plus). TEM (Transmission Electron microscopy) was carried out on a JEOL JEM-3200FS, Field Emission Electron Microscope. The sample preparation of TEM was done by ultrasonication of synthesized samples in ethanol.

Results and discussion

The XRD patterns of all the calcined samples are shown in Fig. 1a, and relative crystallinity results are presented in Table 2. The peaks at 9.4, 12.7, 15.9, 17.8, 27.5, 30.6, 31.3 confirm the formation of the CHA structure of SAPO-34 (Bellatreche et al. 2016; Bakhtiar et al. 2018), but there are also some diffraction peaks at 7.5, 15, 19.8, 21, 22.4 corresponds to the formation of SAPO-5 (Amoozegar et al. 2016; Bakhtiar et al. 2018) which might be because of the composition of templates. The diffraction patterns of S-1 and S-2 shows both phases of SAPO-5 and SAPO-34, but as the time of crystallization escalates, the diffraction peaks of SAPO-34 becomes more prominent for S-3, S-4, S-5. As relative crystallinity is concerned, it increases with time of crystallization for S-1, S-3, S-5, and decreases with the time of crystallization for S-2, S-4, S-6. The sample with the molar ratio of TEAOH/TEA of 0.5 shows a continuous increase in relative crystallinity. EDX results Fig. 7 show that the sample with TEAOH/TEA molar ratio of 0.5 and crystallization time of 8 h, S-6 had comparatively lower Si content than other samples, which might have repercussions on the crystallinity of S-6. For the samples synthesized with TEAOH/TEA molar ratio of 2, the relative crystallinity increased as the result of the formation of the crystalline structure. The pressure formed in the autoclave with the advancement of the crystallization time induces the occurrence of recrystallization. Then there was the breaking of the crystal, which might lead to the decrease in the relative crystallinity. The samples involving TEAOH/TEA of 2 were

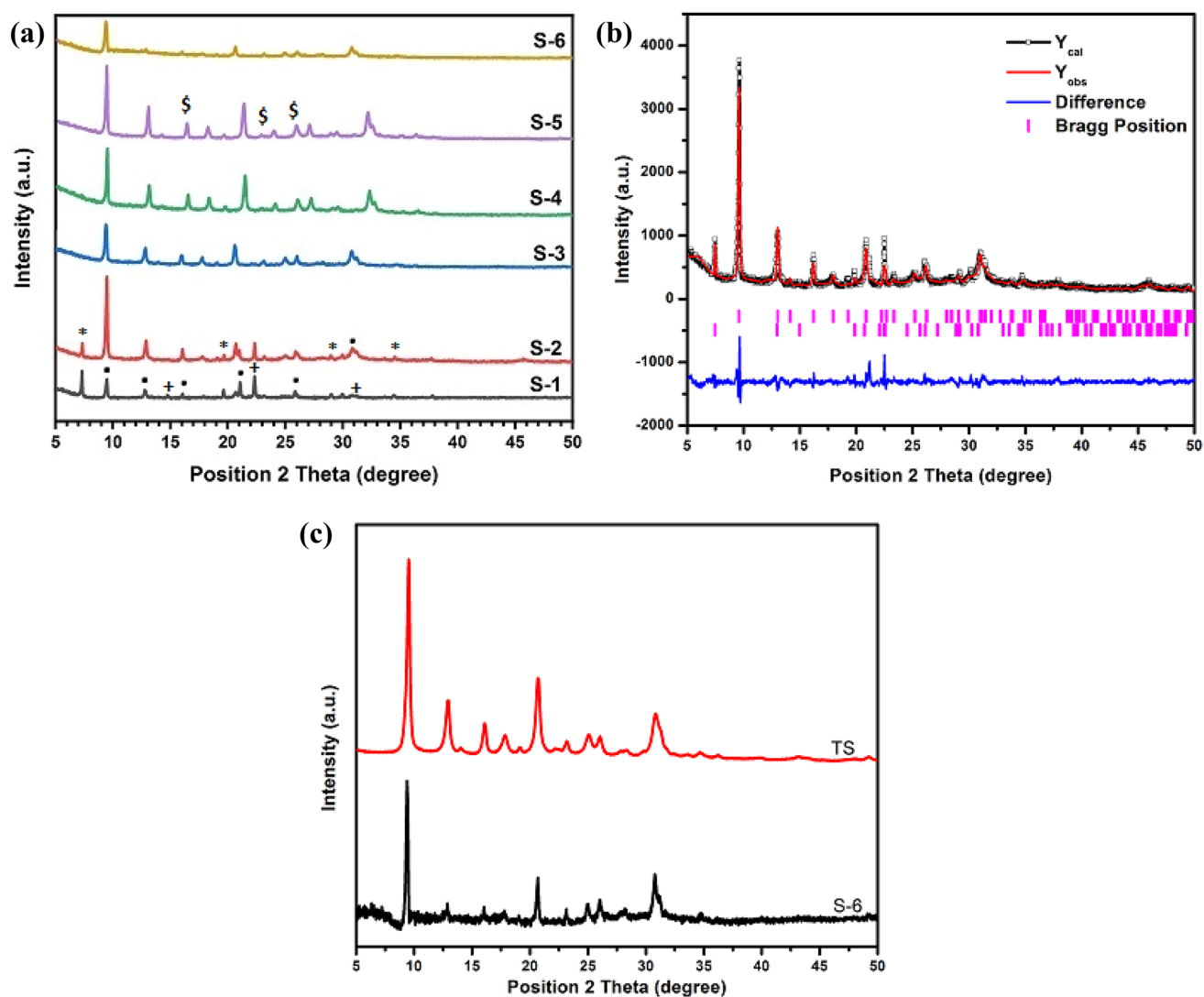


Fig. 1 a XRD patterns of as-synthesized catalyst (S-1, S-2, S-3, S-4, S-5, S-6). b Rietveld refinement of S-2 catalyst. The row of vertical lines in green colour gives the possible Bragg reflection (top to bottom) for SAPO-34 and SAPO-5. c XRD patterns of TS and S-6

Table 2 Relative crystallinity of products

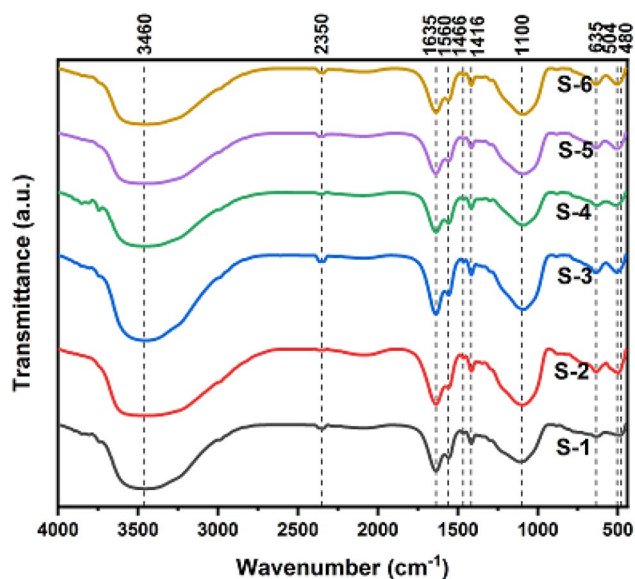
Crystallization time (h)	0.2TEAOH:0.4TEA:0.6Morpholine:0.8DEA	0.4TEAOH:0.2TEA:0.8Morpholine:0.6DEA
3	S-1	S-2
5	S-3	S-4
8	S-5	S-6

an exception as relative crystallinity increases with crystallization time. The reason might be the structural differences arising from the templates concentration. The high relative crystallinity of S-2 shows the faster crystallinity nature of

the synthesis. It has been noted that SAPO-5 disappears at the higher crystallization time, which implies that SAPO-34 is more stable at higher crystallization time. Liu et al. (2012, 2008) suggested that DEA template SAPO-34 has higher crystallinity and silicon content. The diffraction patterns of S-6 and TS in Fig. 1c show that the catalyst prepared by taking moles of TEAOH/TEA as 2, and Morpholine/DEA as 0.75 raises the relative crystallinity of TS to 50% and SAPO-34 is formed. For the Rietveld refinement, the Pseudo Voigt function has been used. Toby's (2006) work on understanding Rietveld refinement is also helpful. The crystallographic information files (CIFs) are referred from the International Zeolite Association, and other CIF are taken from

Table 3 Results of Rietveld refinement

Sample	Phase name	Composition (%v/v)	a(Å)	b(Å)	c(Å)	Alpha (deg)	Beta (deg)	Gamma (deg)	Space group	χ^2
S-1	SAPO-34	54.94	13.60	13.60	14.74	90	90	120	R -3 m (#166)	4.52
	SAPO-5	21.23	13.75	13.75	8.58	90	90	120	P 6/m c c (#192)	
	AlPO ₄	23.83	7.26	7.25	7.17	90	90	90	P-1 (#2)	
S-2	SAPO-34	92.63	13.59	13.59	14.83	90	90	120	R -3 m (#166)	3.69
	SAPO-5	7.37	13.66	13.66	8.58	90	90	120	P 6/m c c (#192)	
S-3	SAPO-34	100	13.95	13.95	14.77	90	90	120	R -3 m (#166)	2.81
S-4	SAPO-34	100	13.68	13.68	14.77	90	90	120	R -3 m (#166)	2.61
S-5	SAPO-34	73.75	13.59	13.59	15.80	90	90	120	R -3 m (#166)	2.29
	Tridymite	26.25	18.55	18.55	8.40	90	90	120	P 63/m c m (#194)	
S-6	SAPO-34	100	13.56	3.56	14.77	90	90	20	R -3 m (#166)	2.98

**Fig. 2** IR- spectr of as-synthesized SAPO samples

the Crystallographic Open Database (Graulis et al. 2009). The parameters like scale factor, cell parameters, FWHM/shape parameters, occupancy, etc., were refined. The order of refinement for all the samples is as follows Background, Scale factor, Instrumental (Zero), Cell parameters, FWHM parameters, Shape parameters, atom coordinates. Table 3 presents the Rietveld refinement results such as percentage

content of phase, lattice parameters of the prepared catalysts. It has been found that there is more than one phase coexisting with the SAPO-34. Figure 1b shows the Rietveld refinement plot of S-2.

FT-IR spectroscopy is mostly employed to establish the framework structure and adsorbed species. The Infrared Spectra of the prepared samples are given in Fig. 2. The characteristic peaks at the wavenumbers of 480, 504, 635, and 1100 cm^{-1} are observed for all the samples, which are similar to the literature (Amoozegar et al. 2016; Mirza et al. 2018; Tan et al. 2002). The peak at 635 cm^{-1} present in all samples shows the bending of the D6 ring, which affirms the formation of the CHA framework (Aghaei and Haghghi 2015). The vibrational feature of the entrapped organic molecules lies in the range of 1700–1200 cm^{-1} (Marchese et al. 1999). The vibrations at 1635 cm^{-1} show the presence of weakly adsorbed water molecules in the SAPO-34 cages (Masoumi and Towfighi 2015). The stretching vibration at 2350 cm^{-1} corresponds to the physical adsorption of CO and CO₂ from the atmosphere (Aghaei and Haghghi 2015). The broad stretching vibration bands at 3200–3600 cm^{-1} are associated with hydroxyl groups such as Si–OH and P–OH tetrahedrally linked with Al, which act as Brønsted acid sites inside the double six rings (Marzpour Shalmani et al. 2017; Mirza et al. 2018).

Substitution of silicon by aluminium or by phosphorous is done by two mechanisms. Replacing phosphorous with

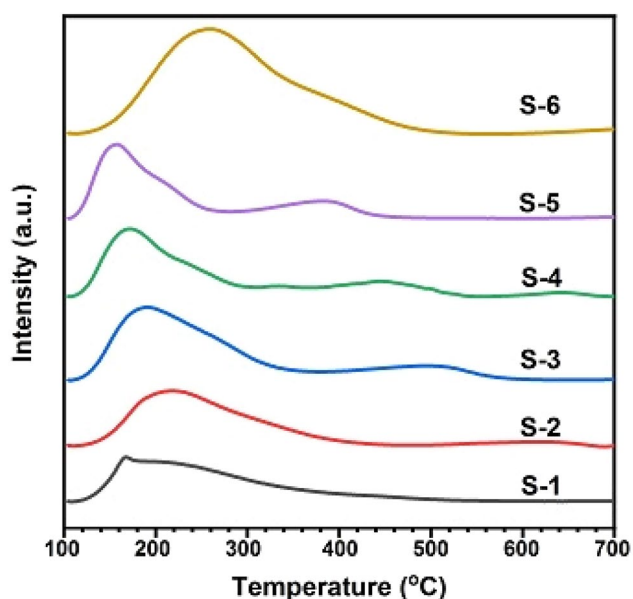


Fig. 3 NH_3 -TPD spectrum of as-synthesized SAPO-34 catalysts

Table 4 TPD test results⁰

Sample	Acid amount (mmol g^{-1}) ^a		
	Total acidity	Weak acid (180–260 °C)	Strong acid (380–600 °C)
S-1	0.82	0.82	–
S-2	0.71	0.67	0.04
S-3	1.02	0.91	0.11
S-4	0.86	0.75	0.11
S-5	1.09	0.92	0.17
S-6	1.30	1.13	0.18

^aCalculated by NH_3 -TPD

silicon generates Brønsted acid sites of bridge hydroxyl groups ($-\text{SiOHAl}-$) which is the first mechanism. The second mechanism is by replacing aluminium and phosphorous with two silicon atoms, which generates no acidic sites but influences the acid centres generated by the first mechanism (Izadbakhsh et al. 2009). NH_3 -TPD (Temperature programmed desorption) was done to measure the number of acid sites, together with the acidic strength of the synthesized catalysts. It has been proven that the incorporation of Si induces acidity in SAPO-34 in AlPO molecular sieves (Borade and Clearfield, 1994). Figure 3 shows the desorption profiles of SAPO-34 (S-1, S-2, S-3, S-4, S-5, and S-6). The two peaks were observed for S-2, S-3, S-4, S-5, except for S-1 and S-6. The first peak of NH_3 (at low temperature)

corresponds to the physical adsorption of NH_3 , and another peak at high-temperature desorption of NH_3 is because of the chemical adsorption of NH_3 . The area under the curve corresponds to the acid site density. The low-temperature desorption peaks are formed because of weak acidic sites, indicate the presence of Si–OH, P–OH, and Al–OH, which is also confirmed by the FT-IR. The strong adsorption peaks at a lower temperature which are possibly weak Brønsted acidic sites were commenced from P–OH groups which are not attached to AlO_4 tetrahedra (Lee et al. 2007; Masoumi and Towfighi 2015). The small intensity peaks of high-temperature desorption might also indicate the Si–OH–Al group Brønsted acidic sites (Amoozegar et al. 2016; Ma et al. 2020; Masoumi and Towfighi 2015). The low-temperature peaks of S-1, S-3, S-4, S-5 were at around the temperature of 180 °C. For S-2 and S-6, the low-temperature peak shifted to around 220 and 280 °C, respectively. The S-1 and S-2 curves resemble the SAPO-5 sample described in the literature (Lee et al. 2007). As observed from Fig. 3 and Table 4, by adding the quadruple templates, there is a lesser formation of more substantial acidity. The effect of four templates on the acidity is not as simple as the addition effect.

Nitrogen adsorption–desorption isotherms are presented in Fig. 4a. The corresponding data for the micropore surface area, total surface area, micropore volume, total volume, and the average pore size are given in Table 5. At the low relative pressure, all the samples exhibit the rapid intake of nitrogen, which indicates the presence of micropores. The non-overlap of adsorption and desorption branches in the case of S-1 and S-2 forms the hysteresis that gives type-IV isotherms, whereas in the case of S-3 and S-4, there is almost coincidence of the adsorption and desorption branches which form the type-I isotherms. The hysteresis loop between $0.4 < p/p_0 < 0.9$ shows the capillary condensation in the mesopores (Marzpour Shalmani et al. 2017). For all the samples, micropore volume is more significant than mesoporous volume except for S-1 and S-6. For the TEAOH/TEA ratio of 0.5, i.e., for samples S-3, S-5 the micropore volume is higher than the mesoporous volume except for sample S-1. For a TEAOH/TEA ratio of 2 except for S-6, the microporous volumes of S-2 and S-4 are higher than the mesoporous volume. This may be due to the distribution of silica that varies with template composition and crystallization time, and impacts the properties of the catalyst. The surface area of all the samples increases with the time of crystallization. The micropore surface area of S-5 is $606 \text{ m}^2/\text{g}$, which has a relative crystallinity of 84%, and the time of crystallization is 8 h. For S-2, the micropore surface area is $462 \text{ m}^2/\text{g}$, and relative crystallinity is 100%. The agglomeration of the particles lowers the crystallinity, resulting in minimal structural

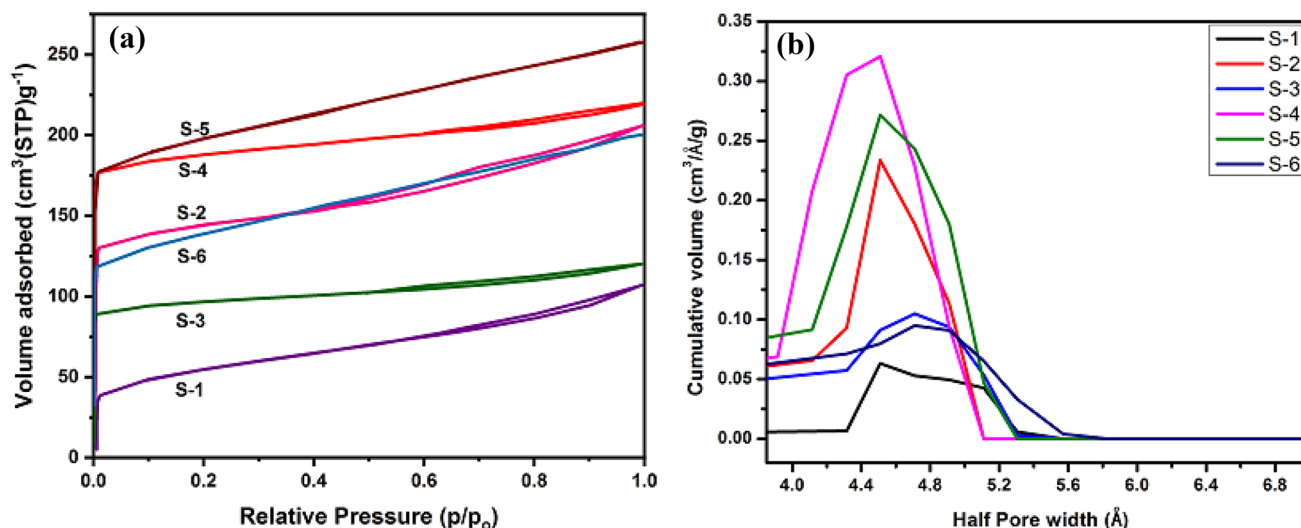


Fig. 4 a Nitrogen adsorption–desorption isotherms of SAPO catalysts. b Pore size distribution of SAPO catalysts

Table 5 The pore structure characteristics of synthesized SAPO-34 samples

Sample	Surface area (m ² /g)		Pore volume (cm ³ /g)		
	S _{micro} ^a	S _{ext} ^a	V _{micro} ^b	V _{meso} ^c	V _{total} ^d
S-1	79	107	0.04	0.11	0.15
S-2	462	105	0.18	0.14	0.32
S-3	350	44	0.13	0.06	0.19
S-4	697	74	0.26	0.09	0.35
S-5	606	173	0.23	0.18	0.41
S-6	352	175	0.14	0.17	0.31

^aS_{ext} (external surface area) and S_{micro} (micropore surface area) are calculated by the t-plot method

^bV_{micro} (Micropore volume) is calculated by the t-plot method

^cV_{meso} (Mesopore volume) is calculated by using the BJH (Barrett-Joyne-Halenda) method (from desorption)

^dV_{total} is total pore volume at P/P₀ > 0.97

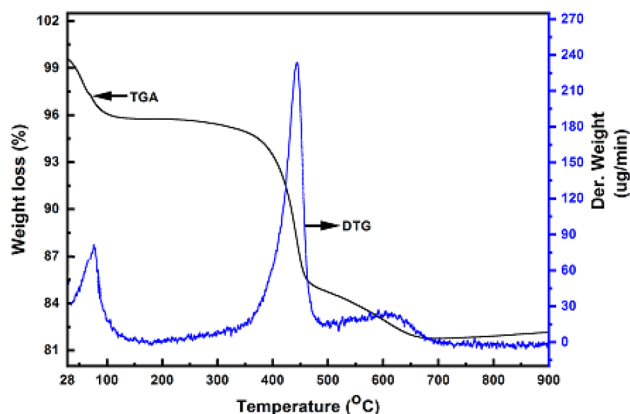


Fig. 5 TGA–DTG profile of S-4

pores, which further shrink the rate of diffusion and amount of adsorbate molecule into the channel of the crystallites, thus reducing the surface area (Izadbakhsh et al. 2009). Figure 4b shows the DFT pore size distribution of the as-synthesized samples. The half pore width of all the samples is concentrated in the narrow micropores range.

Thermogravimetric analysis is done to verify the incorporation of the template molecule in the structure of the samples and their complete removal after calcination. Calcination is a preliminary step before the catalyst is used as an adsorbent or catalyst in any application. The TGA-DTG curve of S-4 is shown in Fig. 5. Weight loss is divided into three steps. Weight loss until 200 °C is 4.2% and is attributed to the removal of water. There is a sharp decrease in the second weight loss between 200 and 466 °C, which is 10% and related to the decomposition of the template. The final gradual weight loss (> 466 °C) is 3.2%, which is probably attributed to the removal of remaining template residues in the channel and cages of the sample. The peaks of DTG curves show three-step weight losses for the removal of organic molecules.

Figure 6a shows the SEM micrographs of the as-synthesized catalyst. All the SEM micrographs show the formation of agglomeration of cubic-rhombohedral morphology (Hirota et al. 2010), which resembles natural chabasite except the samples S-1 and S-2. SEM micrographs of S-1 and S-2 show the initiation of the creation of the cubic particles. The XRD patterns of S-1 and S-2 affirm the existence of SAPO-5 structures, which are not recognized by hexagonal like structure in Fig. 6, which may be because of the insignificant generation of SAPO-5 impurity phase. With the increase in crystallization time, the impurity phase decreases, and crystals appear. For S-3, S-4, S-5, and S-6,

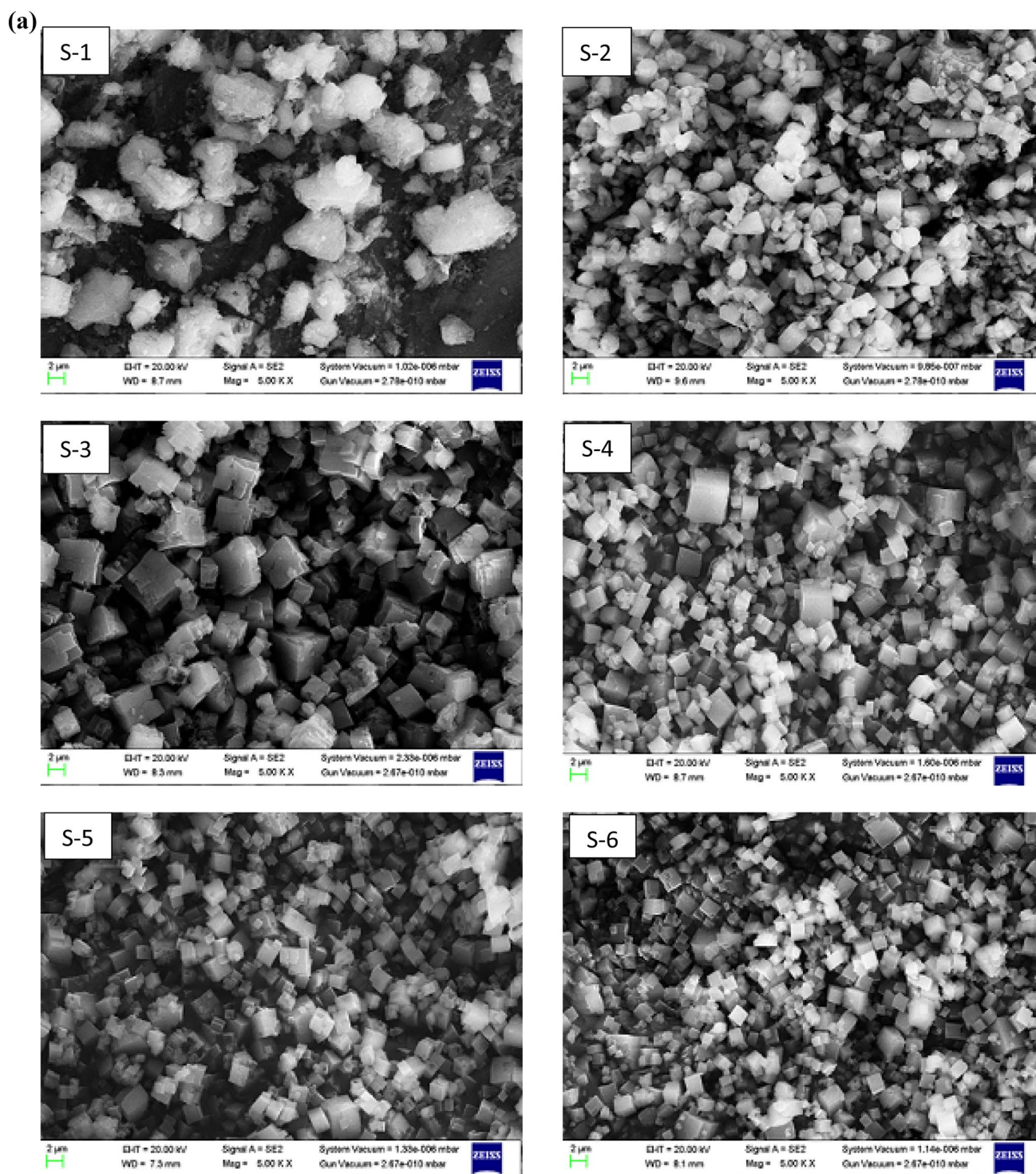


Fig. 6 a SEM images of as-synthesized SAPO-34 catalysts. b Particle size distribution of the SAPO catalysts

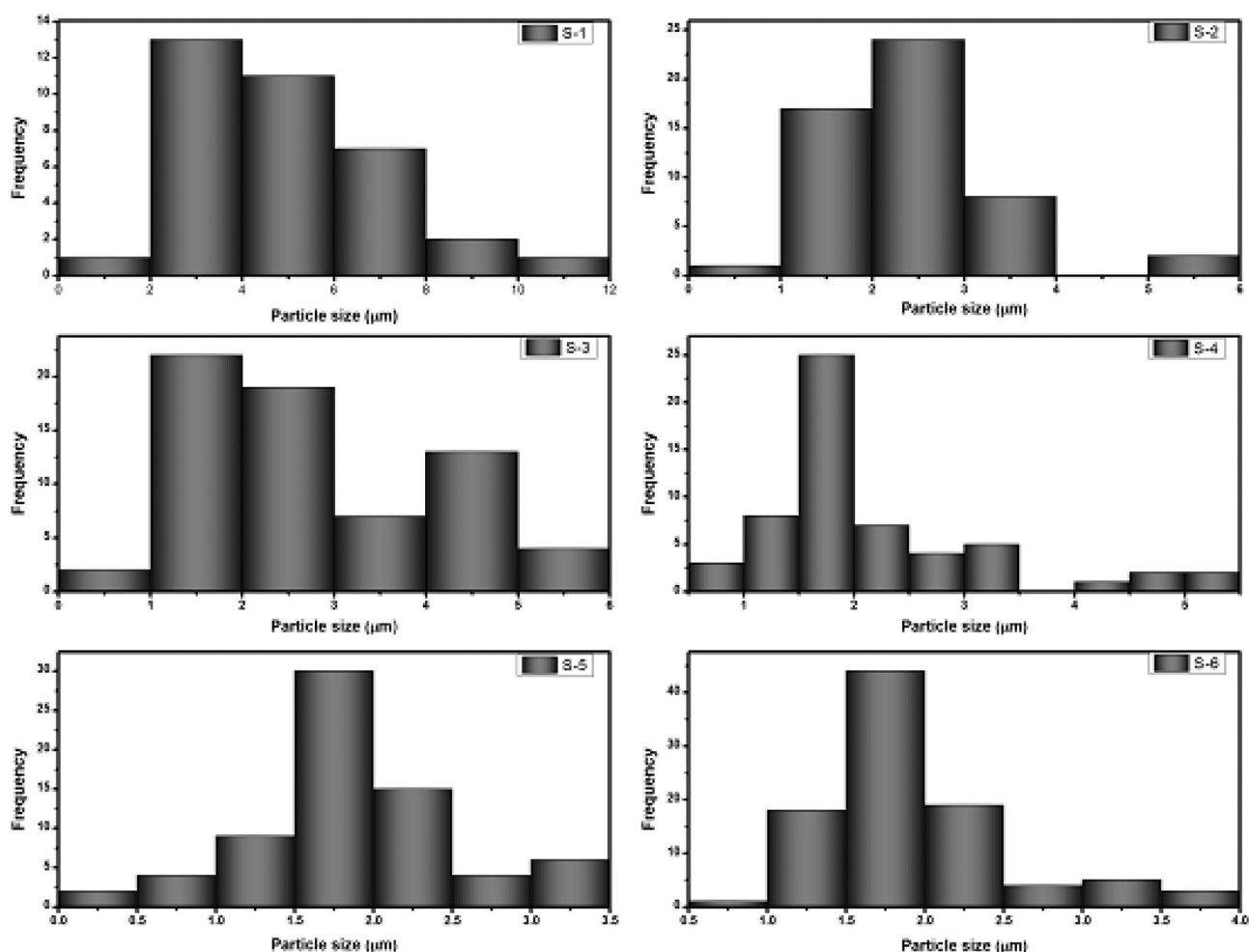


Fig. 6 (continued)

smoothness and crystal size vary though their cubical shapes are similar. Particle size histograms are presented in Fig. 6b. For S-1 and S-2, the particle size varies between 2 and 11 μm and 1–5.5 μm , respectively. The average particle size of S-3 is 2.8 μm , and for S-4, S-5 and S-6 are nearly 2 μm .

The composition of Si, Al, P, and O are studied by EDX and are given in Fig. 7. The dot mapping images show the symmetrical distribution of all the elements used to synthesize the catalyst. The dispersion of Si is maximum in the case of S-5, and it is slightly less for S-4. This might indicate that the distribution of silica has the most significant effect on the catalytic properties of the SAPO-34.

TEM images of S-3, S-4, S-5, and S-6 are shown in Fig. 8 (Liu et al. 2016). It is noticed that thin plates are attached with the cubical particles in the case of S-4, S-5, and S-6. The production of a hundred nanometer-sized particles along with the larger particle size can be clearly seen from the

corresponding TEM images. The particle size of the cubes varies from 700 to 1000 nm. In the case of S-3, the cube is dense, which may be because of high Si content. TEM images are also consistent with the SEM images. For S-1 and S-2, no proper morphology is obtained.

Conclusion

Advancement of SAPO-34 has been an area of research for scientists in recent years because of the remarkable properties suitable for catalytic reactions. The present work contributes to previous researches by combining the four templates and the successful synthesis of SAPO-34 in comparatively less duration of crystallization time. The dry gel method embraces high nucleation, and a low growth rate directs the full crystallization of the catalyst. The change in

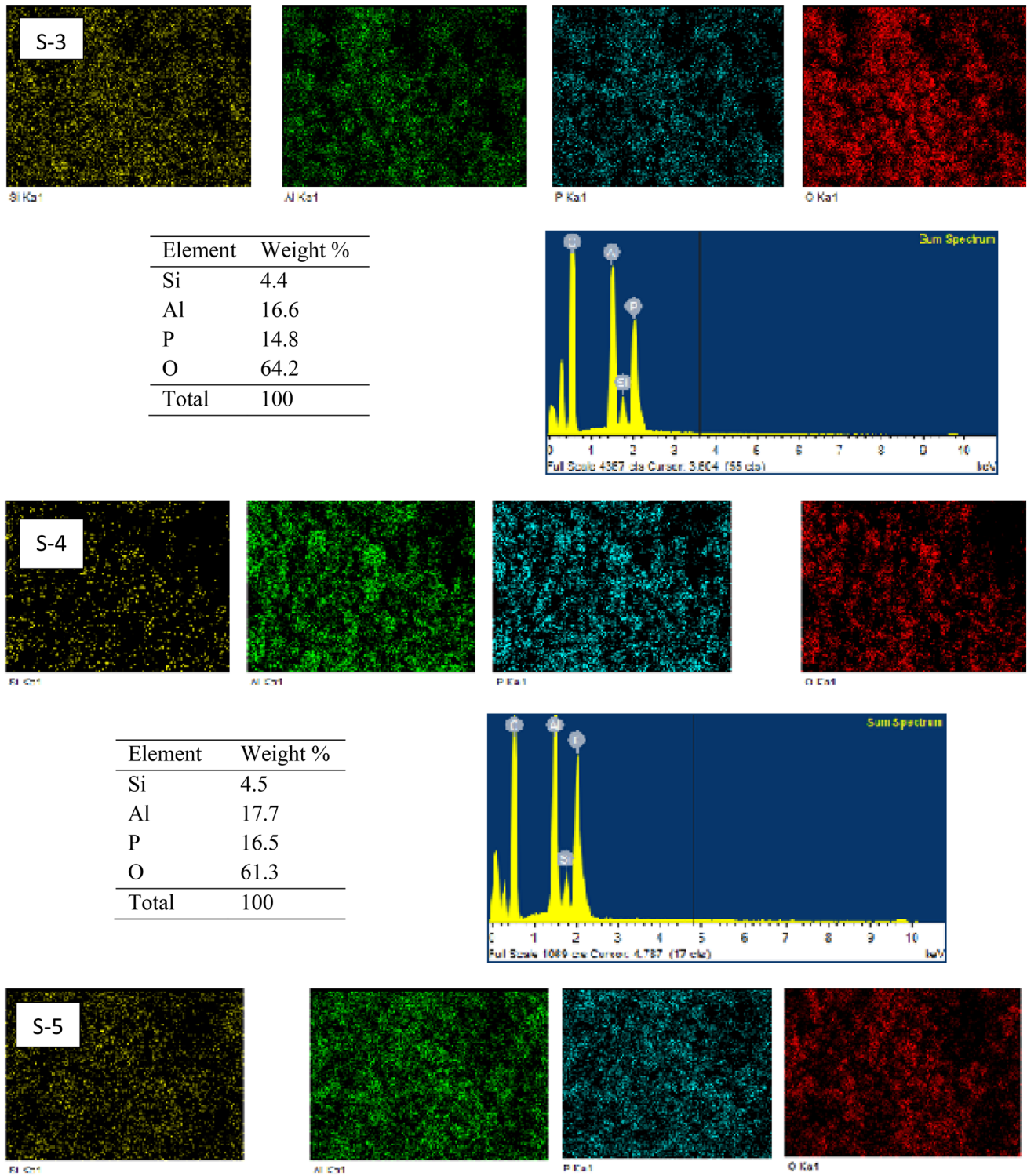
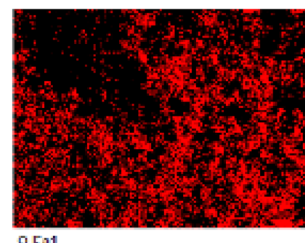
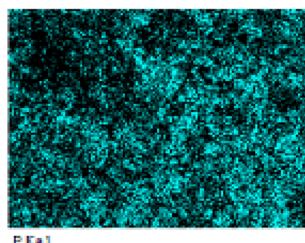
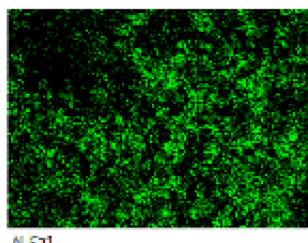
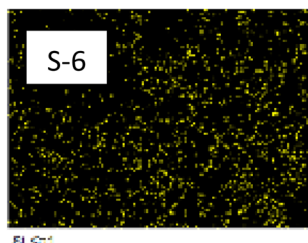
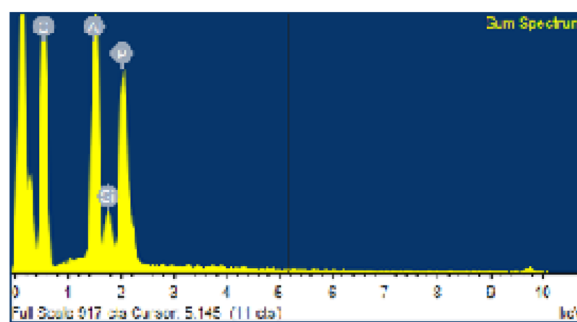


Fig. 7 EDX dot mapping and elemental composition of S-3, S-4, S-5 and S-6

Element	Weight %
Si	4.8
Al	18.0
P	15.7
O	61.5
Total	100



Element	Weight %
Si	4.3
Al	18.6
P	16.9
O	60.2
Total	100

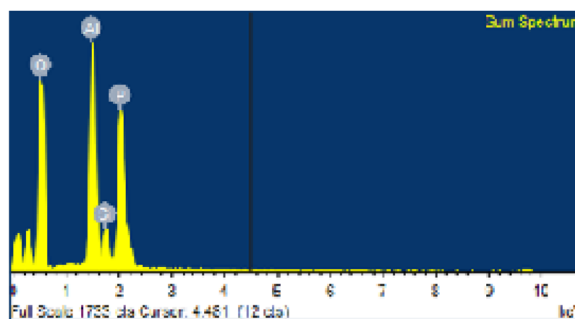
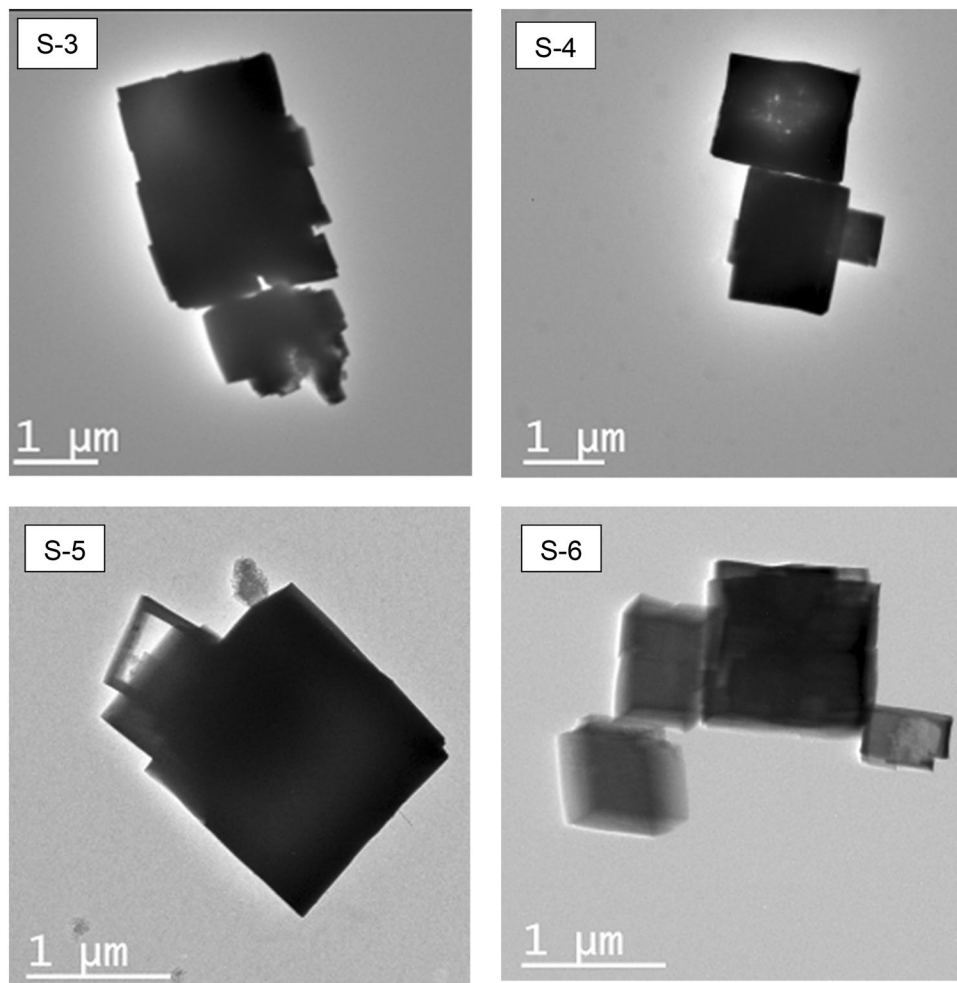


Fig. 7 (continued)

crystallinity, acidity, and morphology is obtained by varying the moles of templates and also by the crystallization time. The synthesized sample characterized by analytical techniques enlightens the understanding of the formation of SAPO-34. XRD results show that S-2 is more crystalline than all the samples but has impurity of SAPO-5. S-5 and S-4 are more crystalline than S-1, S-3. It can be noted from the X-ray diffraction patterns and EDX results that the TEAOH/TEA ratio of 0.5 at the crystallization time of 8 h (S-6) led to the impure phase, which might be because of the poor distribution of silica. It can be concluded that a higher TEA amount and crystallization time reduce the proper generation of the SAPO-34 framework. The crystallinity of TS proves that DEA also plays an important role. EDX results show that Si contents for S-3 and S-5 increased, which may

be because of the DEA content present in the catalyst. The characteristic peaks of SAPO-34 are observed in the Fourier Transform IR spectra. The acidity of S-6 and S-5 is highest, as shown by NH_3 -TPD curves. The micropore surface area of S-4 and S-5 is higher among all the synthesized samples. Thermal analysis (TGA) shows the proper removal of the organic templates. SEM micrographs show the cubic morphology in the samples synthesized at the time of crystallization of 5 and 8 h, that is, S-3, S-4, S-5, and S-6. For the generation SAPO-34 molecular sieve, catalyst template combination and crystallization time are very crucial. By considering the above results, we can confirm that crystallization time in the case of the dry gel method leads to more recognizable crystallinity, morphology, acidity, and the surface area of the SAPO-34.

Fig. 8 TEM images of S-3, S-4, S-5, and S-6



Acknowledgements The author would like to thank the Ministry of Human Resource Research Development (MHRD), Government of India for financial assistantship. The author would also like to sincerely thank Prof. Shishir Sinha (Department of Chemical Engineering, IIT Roorkee) and Prof. Surendra Kumar (Former Professor, Department of Chemical Engineering, IIT Roorkee) for the prolific discussions.

Funding Not applicable.

Availability of data Not applicable.

Declarations

Conflict of interest We have no conflicts of interest to disclose.

References

- Aghaei E, Haghghi M (2015) High temperature synthesis of nanostructured Ce-SAPO-34 catalyst used in conversion of methanol to light olefins: effect of temperature on physicochemical properties and catalytic performance. *J Porous Mater* 22:187–200. <https://doi.org/10.1007/s10934-014-9885-5>
- Ahmad NNR, Leo CP, Ahmad AL (2019) Effects of solvent and ionic liquid properties on ionic liquid enhanced polysulfone/SAPO-34 mixed matrix membrane for CO₂ removal. *Microporous Mesoporous Mater* 283:64–72. <https://doi.org/10.1016/j.micromeso.2019.04.001>
- Álvaro-Muñoz T, Marquez-Alvarez C, Sastre E (2012) Use of different templates on SAPO-34 synthesis: Effect on the acidity and catalytic activity in the MTO reaction. *Catal Today* 179:27–34. <https://doi.org/10.1016/j.cattod.2011.07.038>
- Amoozegar A, Haghghi M, Aghamohammadi S (2016) Enhancement of catalytic properties and lifetime of nanostructured SAPO-34 by La isomorphous substitution and alteration of Si/Al ratio used in methanol conversion to light olefins. *RSC Adv* 6:51024–51036. <https://doi.org/10.1039/c6ra02664h>
- Askari S, Halladj R (2012) Ultrasonic pretreatment for hydrothermal synthesis of SAPO-34 nanocrystals. *Ultrason Sonochem* 19:554–559. <https://doi.org/10.1016/j.ultsonch.2011.09.006>
- Askari S, Sedighi Z, Halladj R (2014) Rapid synthesis of SAPO-34 nanocatalyst by dry gel conversion method templated with morpholine: Investigating the effects of experimental parameters. *Microporous Mesoporous Mater* 197:229–236. <https://doi.org/10.1016/j.micromeso.2014.06.028>
- Bahrami H, Darian JT, Sedighi M (2018) Simultaneous effects of water, TEAOH and morpholine on SAPO-34 synthesis and its

- performance in MTO process. *Microporous Mesoporous Mater* 261:111–118. <https://doi.org/10.1016/j.micromeso.2017.11.011>
- Bakhtiar S ul H, Ali S, Dong Y, Wang X, Yuan F, Li Z, Zhu Y (2018) Selective synthesis of the SAPO-5 and SAPO-34 mixed phases by controlling Si/Al ratio and their excellent catalytic methanol to olefins performance. *J Porous Mater* 25:1455–1461. <https://doi.org/10.1007/s10934-018-0558-7>
- Bellatreche S, Hasnaoui A, Boukoussa B, García-Aguilar J, Berenguer-Murcia Á, Cazorla-Amoros D, Bengueddach A (2016) Structural and textural features of TiO₂/SAPO-34 nanocomposite prepared by the sol–gel method. *Res Chem Intermed* 42:8039–8053. <https://doi.org/10.1007/s11164-016-2577-9>
- Borade RB, Clearfield A (1994) A comparative study of acidic properties of SAPO-5, -11, -34 and -37 molecular sieves. *J Mol Catal* 88:249–265. [https://doi.org/10.1016/0304-5102\(93\)E0262-F](https://doi.org/10.1016/0304-5102(93)E0262-F)
- Doan T, Nguyen K, Dam P, Vuong TH, Le MT, Thanh HP (2019) Synthesis of SAPO-34 using different combinations of organic structure-directing agents. *J Chem* 2019:1–10. <https://doi.org/10.1155/2019/6197527>
- Dumitriu E, Azzouz A, Hulea V, Lutic D, Kessler H (1997) Synthesis, characterization and catalytic activity of SAPO-34 obtained with piperidine as templating agent. *Microporous Mater* 10:1–12. [https://doi.org/10.1016/S0927-6513\(96\)00107-1](https://doi.org/10.1016/S0927-6513(96)00107-1)
- Fan D, Tian P, Xu S, Wang D, Yang Y, Li J, Wang Q, Yang M, Liu Z (2016) SAPO-34 templated by dipropylamine and diisopropylamine: synthesis and catalytic performance in the methanol to olefin (MTO) reaction. *New J Chem* 40:4236–4244. <https://doi.org/10.1039/C5NJ02351C>
- Fan J, Ning P, Wang Y, Song Z, Liu X, Wang H, Wang J, Wang L, Zhang Q (2019) Significant promoting effect of Ce or La on the hydrothermal stability of Cu-SAPO-34 catalyst for NH₃-SCR reaction. *Chem Eng J* 369:908–919. <https://doi.org/10.1016/j.cej.2019.03.049>
- Graulis S, Chateigner D, Downs RT, Yokochi AFT, Quirós M, Lutterotti L, Manakova E, Butkus J, Moeck P, Le Bail A (2009) Crystallography open database - an open-access collection of crystal structures. *J Appl Crystallogr* 42:726–729. <https://doi.org/10.1107/S0021889809016690>
- Hirota Y, Murata K, Tanaka S, Nishiyama N, Egashira Y, Ueyama K (2010) Dry gel conversion synthesis of SAPO-34 nanocrystals. *Mater Chem Phys* 123:507–509. <https://doi.org/10.1016/j.matchemphys.2010.05.005>
- Izadbakhsh A, Farhadi F, Khorasheh F, Sahebdehghani S, Asadi M, Yan ZF (2009) Key parameters in hydrothermal synthesis and characterization of low silicon content SAPO-34 molecular sieve. *Microporous Mesoporous Mater* 126:1–7. <https://doi.org/10.1016/j.micromeso.2008.12.009>
- Lee YJ, Baek SC, Jun KW (2007) Methanol conversion on SAPO-34 catalysts prepared by mixed template method. *Appl Catal A Gen* 329:130–136. <https://doi.org/10.1016/j.apcata.2007.06.034>
- Liang J, Li H, Zhao S, Guo W, Wang R, Ying M (1990) Characteristics and performance of SAPO-34 catalyst for methanol-to-olefin conversion. *Appl Catal* 64:31–40. [https://doi.org/10.1016/S0166-9834\(00\)81551-1](https://doi.org/10.1016/S0166-9834(00)81551-1)
- Liu G, Tian P, Zhang Y, Li J, Xu L (2008) Synthesis of SAPO-34 templated by diethylamine: crystallization process and Si distribution in the crystals. *Microporous Mesoporous Mater* 114:416–423. <https://doi.org/10.1016/j.micromeso.2008.01.030>
- Liu G, Tian P, Liu Z (2012) Synthesis of SAPO-34 molecular sieves templated with diethylamine and their properties compared with other templates. *Chinese J Catal* 33:174–182. [https://doi.org/10.1016/s1872-2067\(11\)60325-2](https://doi.org/10.1016/s1872-2067(11)60325-2)
- Liu X, Ren S, Zeng G, Liu G, Wu P, Wang G, Chen X, Liu Z, Sun Y (2016) Coke suppression in MTO over hierarchical SAPO-34 zeolites. *RSC Adv* 6:28787–28791. <https://doi.org/10.1039/c6ra02282k>
- Lok BM, Cannan TR, Messina CA (1983) The role of organic molecules in molecular sieve synthesis. *Zeolites* 3:282–291. [https://doi.org/10.1016/0144-2449\(83\)90169-0](https://doi.org/10.1016/0144-2449(83)90169-0)
- Lok BM, Messina CA, Cannan TR, Flanigen EM (1984a) Silicoaluminophosphate molecular sieves: another new class of microporous crystalline inorganic solids. *J Am Chem Soc* 106:6092–6093. <https://doi.org/10.1021/ja00332a063>
- Lok BM, Messina CA, Patton RL, Gajek RT, Cannan TR, Flanigen EM (1984) United States Patent
- Ma Y, Wu X, Liu L, Cao L, Ran R, Si Z, Gao F, Weng D (2020) Critical roles of Cu(OH)₂ in low-temperature moisture-induced degradation of Cu-SAPO-34 SCR catalyst: Correlating reversible and irreversible deactivation. *Appl Catal B Environ* 278:119306. <https://doi.org/10.1016/j.apcatb.2020.119306>
- Marchese L, Frache A, Gianotti E, Martra G, Causa M, Coluccia S (1999) ALPO-34 and SAPO-34 synthesized by using morpholine as templating agent. FTIR and FT-Raman studies of the host–guest and guest–guest interactions within the zeolitic framework. *Microporous Mesoporous Mater* 30:145–153. [https://doi.org/10.1016/S1387-1811\(99\)00023-2](https://doi.org/10.1016/S1387-1811(99)00023-2)
- Marzpour Shalmani F, Halladj R, Askari S (2017) Physicochemical characterization to assess Ni and Zn incorporation into zeolite SAPO-34 nanoparticles synthesized with different mixing methods through ultrasound-promoted crystallization. *RSC Adv* 7:26756–26769. <https://doi.org/10.1039/c7ra00272f>
- Masoumi S, Towfighi J (2015) Characterization and optimization of SAPO-34 catalysts synthesized by mixed templates in MTO reaction. *Iran J Chem Eng* 12:4–14
- Masoumi S, Towfighi J, Mohamadizadeh A, Kooshki Z, Rahimi K (2015) Tri-templates synthesis of SAPO-34 and its performance in MTO reaction by statistical design of experiments. *Appl Catal A Gen* 493:103–111. <https://doi.org/10.1016/j.apcata.2014.12.033>
- Mirza K, Mohammad G, Mohammad H, Afghan A (2018) Hydrothermal synthesis of modified Fe, Ag and K-SAPO-34 nanostructured catalysts used in methanol conversion to light olefins. *Microporous Mesoporous Mater* 260:155–165. <https://doi.org/10.1016/j.micromeso.2017.10.045>
- Najafi N, Askari S, Halladj R (2014) Hydrothermal synthesis of nano-sized SAPO-34 molecular sieves by different combinations of multi templates. *Powder Technol* 254:324–330. <https://doi.org/10.1016/j.powtec.2014.01.037>
- Nishiyama N, Kawaguchi M, Hirota Y, Van Vu D, Egashira Y, Ueyama K (2009) Size control of SAPO-34 crystals and their catalyst lifetime in the methanol-to-olefin reaction. *Appl Catal A Gen* 362:193–199. <https://doi.org/10.1016/j.apcata.2009.04.044>
- Popova M, Minchev C, Kanazirev V (1998) Methanol conversion to light alkenes over SAPO-34 molecular sieves synthesized using various sources of silicon and aluminium. *Appl Catal A Gen* 169:227–235. [https://doi.org/10.1016/S0926-860X\(98\)00003-9](https://doi.org/10.1016/S0926-860X(98)00003-9)
- Prakash AM, Unnikrishnan S (1994) Synthesis of SAPO-34: High Silicon Incorporation in the Presence of Morpholine as Template. *J Chem Soc Faraday Trans* 90:2291–2296. <https://doi.org/10.1039/FT9949002291>
- Rostami RB, Ghavipour M, Behbahani RM, Aghajafari A (2014) Improvement of SAPO-34 performance in MTO reaction by utilizing mixed-template catalyst synthesis method. *J Nat Gas Sci Eng* 20:312–318. <https://doi.org/10.1016/j.jngse.2014.07.015>
- Sánchez-Sánchez M, Romero AÁ, Irene P-H, Sastre E (2017) Ionothermal preparation of triclinic SAPO-34 and its catalytic performance in the MTO process. *Catal Today* 296:239–246. <https://doi.org/10.1016/j.cattod.2017.04.065>
- Sedighi M, Bahrami H, Towfighi Darian J (2014) Thorough investigation of varying template combinations on SAPO-34 synthesis, catalytic activity and stability in the methanol conversion to light olefin. *RSC Adv* 4:49762–49769. <https://doi.org/10.1039/c4ra08607d>

- Shalmani FM, Halladj R, Askari S (2012) Effect of contributing factors on microwave-assisted hydrothermal synthesis of nanosized SAPO-34 molecular sieves. *Powder Technol* 221:395–402
- Sun C, Wang Y, Hengbao C, Wang X, Wang C, Zhang X (2020) Seed-assisted synthesis of hierarchical SAPO-18/34 intergrowth and SAPO-34 zeolites and their catalytic performance for the methanol-to-olefin reaction. *Catal Today* 355:188–198. <https://doi.org/10.1016/j.cattod.2019.04.038>
- Tan J, Liu Z, Bao X, Liu X, Han X, He C, Zhai R (2002) Crystallization and Si incorporation mechanisms of SAPO-34. *Microporous Mesoporous Mater* 53:97–108. [https://doi.org/10.1016/S1387-1811\(02\)00329-3](https://doi.org/10.1016/S1387-1811(02)00329-3)
- Toby BH (2006) R factors in Rietveld analysis: How good is good enough? *Powder Diffr* 21:67–70. <https://doi.org/10.1154/1.2179804>
- Valizadeh B, Askari S, Halladj R, Haghmoradi A (2014) Effect of synthesis conditions on selective formation of SAPO-5 and SAPO-34. *Synth. React. Inorganic. Met Nano-Metal Chem* 44:79–83. <https://doi.org/10.1080/15533174.2013.768646>
- Vomscheid R, Briend M, Peltre MJ, Man PP, Barthomeuf D (1994) The role of the template in directing the Si distribution in SAPO zeolites. *J Phys Chem* 98:9614–9618. <https://doi.org/10.1021/j100089a041>
- Wang Q, Wang L, Wang H, Li Z, Wu H, Li G, Zhang X, Zhang S (2011) Synthesis, characterization and catalytic performance of SAPO-34 molecular sieves for methanol-to-olefin (MTO). *Asia-Pacific J Chem Eng* 6:596–605. <https://doi.org/10.1002/apj.453>
- Wang P, Lv A, Hu J, Lu G (2012) The synthesis of SAPO-34 with mixed template and its catalytic performance for methanol to olefins reaction. *Microporous Mesoporous Mater* 152:178–184. <https://doi.org/10.1016/j.micromeso.2011.11.037>
- Wilson ST, Lok BM, Messina CA, Cannan TR, Flanigen EM (1982) Aluminophosphate molecular sieves: a new class of microporous crystalline inorganic solids. *J Am Chem Soc* 104:1146–1147. <https://doi.org/10.1021/ja00368a062>
- Wu T, Lucero J, Crawford JM, Sinnwell MA, Thallapally PK, Carreon MA (2019) SAPO-34 membranes for xenon capture from air. *J Memb Sci* 573:288–292. <https://doi.org/10.1016/j.memsci.2018.12.021>
- Ye L, Cao F, Ying W et al (2001) Effect of different TEOH / DEA combinations on SAPO-34.s synthesis and catalytic performance. *J Porous Mater.* 18:225–232. <https://doi.org/10.1007/s10934-010-9374-4>
- Zong Z, Carreon MA (2017) Thin SAPO-34 membranes synthesized in stainless steel autoclaves for N₂/CH₄ separation. *J Memb Sci* 524:117–123. <https://doi.org/10.1016/j.memsci.2016.11.011>

Publisher's Note Springer Nature remains neutral with regard to jurisdictional claims in published maps and institutional affiliations.